

IDRCNN: A Novel Deep Learning Network Model for Pancreatic Ductal Adenocarcinoma Detection on Computed Tomography

Original Scientific Paper

K. Laxminarayananamma

Department of Information Technology, Institute of Aeronautical Engineering,
Hyderabad 500043, India
k.laxminarayananamma@iare.ac.in

R.V. Krishnaiah

Electronics and Communication Engineering, Chebrolu Engineering College,
Chebrolu (Vi & Md)-522212, Guntur, Andhra Pradesh, India
principal@rvit.edu.in

P. Sammulal

Computer Science and Engineering, JNTUH, Kondagattu,
Karimnagar, Jagtial, Telangana 505501, India.
sam@jntuh.ac.in

Abstract – Early identification of pancreatic ductal adenocarcinoma (PDAC) improves prognosis. Still, it is difficult since lesions are generally smaller and difficult to define on contrast-enhanced computed tomography images (CE-CT). Ineffective PDAC diagnosis has recently been achieved using deep learning models, but the output localized and identified images are of poor quality. This research focuses on small lesions and presents a new, efficient automatic deep-learning network model for PDAC detection. The Improved Deep Residual Convolutional Neural Network (IDRCNN) detects PDAC. The hyperparameter is optimized using the Tunicate Swarm Optimization Algorithm (TSOA) algorithm. A better diagnosis is made due to segmenting the surrounding anatomy structure effects, such as PD. We train a proposed IDRCNN model for segmenting and detecting lesions automatically using CE-CT images. Two more IDRCNN models are trained with the aim of investigating the effects of anatomy integration: (i) segmentation of tumor and pancreas (IDRCNN_TP), and (ii) segmentation of pancreatic Duct (IDRCNN_PD). The three networks' performance was assessed using an external, publicly available test set. Due to its effective classification results, the proposed method produces improved identification results for automated preliminary diagnosis of PDAC in cervical cancer clinics and hospitals. The performance of the proposed method is evaluated using a publicly assessable CT image dataset. It outperforms the existing state-of-the-art methods and achieved 98.67% accuracy, 97.26% recall, 98.52% precision, 97.65% sensitivity, and 98.45% specificity for pancreatic tumor detection.

Keywords: computed tomography, deep learning, surrounding anatomy, and PDAC detection

1. INTRODUCTION

The most prevalent kind of pancreatic cancer is pancreatic ductal adenocarcinoma (PDAC). It has the poorest prognosis among all cancers globally [1, 2]. Pancreatic cancer is becoming more common, and by 2030, it is anticipated to surpass lung carcinoma as the second-most common reason for cancer-related deaths in Western societies. [3, 4]. Patients with early disease stages have a significantly higher 3-year survival rate (82%) than other patient groups [5]. At the time of diagnosis, about 80–85% of patients had either metastatic or resectable disease since early detection of tumors

is extremely rare [6, 7]. These facts clearly show that improving patient outcomes requires the early identification of PDAC [8, 9].

Early PDAC detection is difficult because most patients exhibit particular symptoms in the late stages of the illness, and a general population screening is prohibitively expensive with currently available technology [10]. Additionally, PDAC tumors are challenging to see on CT scans, the preferred method for early diagnosis, as the lesions have asymmetrical shapes and ill-defined margins [11]. This presents a considerably greater issue in the disease's early stages because lesions are

frequently iso-attenuating and tiny (2 cm), making them readily missed even by seasoned radiologists [12, 13]. According to a new study that tracked the course of pre-diagnostic PDAs' CT alterations, suspicious abnormalities could have been noticed 18 to 12 months earlier [14]. However, just 44% of patients were referred for additional study by radiologists because they were ineffective at spotting those alterations [15].

By utilizing large volumes of imaging data, artificial intelligence (AI) can help radiologists discover PDAC early [16]. CNNs are a subgroup especially effective at analyzing images among deep learning models. Using images has proven to be accurate in detecting numerous types of cancer [17]. The significant features of the images are extracted by using CNN after completing the process of a series of convolution and pooling for diagnosis [18].

In the input image, clinically useful computer-aided diagnostic tools should be able to locate the lesion and, if cancer is present, determine its existence with relatively little user involvement [19]. Deep learning methods are now being researched in diagnosing PDAC automatically [20]. However, several investigations only accomplish the binary classification without associated lesion location. We developed a more effective deep-learning model for accurate PDAC lesion detection and localization in this research. We provide a completely automated deep-learning method; it produces highly accurate segmented tumor images in the result using abdominal CE-CT images. Additionally, we investigate the effects of integrating the surrounding anatomy.

The main contribution of the research is

- A segmentation-oriented approach is proposed in the present research on the process of PDAC diagnosis. The diagnosis and segmentation of PDAC are made using a new, effective deep learning-based IDRCNN model.
- For the detection and localization of PDAC, three distinct IDRCNN models were trained in this research: (1) Tumor segmentation (IDRCNN_T), (2) Tumor and Pancreas segmentation (IDRCNN_TP), and (3) Pancreatic Duct segmentation (IDRCNN_PD).
- The hyper-parameters of the networks are optimized by using TSOA. The hyper-parameters of the proposed network model, such as the number of iterations, position angle, wide angle, population size, and end condition, are effectively updated by this optimization algorithm. This proposed network produced results with greater accuracy in the diagnosis of PDAC.
- The proposed method is evaluated on publicly accessible datasets. The experiments are performed on the Python platform. According to the experimental data, the proposed approach outperforms the state efficiency concerning all other approaches.

The structure of the presented research is as follows: related prior research is shown and discussed in Sec-

tion 2. Section 3 provides a detailed explanation of the proposed methodology. The experimental findings and discussions are presented in Section 4. Finally, Section 5 provides conclusions of the present research.

2. RELATED PRIOR WORKS

For PDAC detection, we review some recent deep-learning models in this section. For the segmentation of pancreatic histopathological images, the first deep convolutional neural network architecture was developed by Fu et al. [21]. The two stages, including the WSI level and patch level, are used for the training process, and it is built on a two-step framework based on various recognizing objects. The hidden features for the patch-level classification are extracted from the training set using the CNN model. The cancer regions are predicted and located using the U-Net for patch-level segmentation.

A new model was created by Qureshi et al. [22] to categorize people at high risk for PDAC by automatically recognizing pre-diagnostic CT images. Using radiomic analysis of images from the internal dataset, numerous characteristics that could be used as PDAC predictors were discovered. The identified predictors were then used to train the Naive Bayes classifier, automatically classifying CT scans into groups of healthy controls or pre-diagnostic individuals.

For PDAC mass and surrounding vessel segmentation in CT images, an approach based on CNN was presented by Mahmoudi et al. [23] while also integrating potent traditional features. Using the original image's 3D Local Binary Pattern (LBP) map, the pancreas region is first localized from the entire CT volume. Then, Texture Attention U-Net (TAU-Net) is used to segment PDAC mass. The benefits of both networks are then added together using a 3D-CNN ensemble model.

Transfer learning was utilized by Zhang et al. [24] to develop a CNN model for feature extraction from CT images. According to this study, most radiomics and transfer learning features show only marginally positive linear associations, indicating that these two feature sets may be complementary. Additionally, we evaluated feature fusion techniques to examine their predictive ability for overall survival.

A PDAC resection specimen's discrete cellularity regions were examined by Jungmann et al. [25] using standard histopathology procedures. Iodine concentrations and regional tumor cellularity were matched, as were Hounsfield Units obtained from CT scans. The association between various levels of cellularity in traditional iodine map reconstructions and virtual monoenergetic is assessed using one-way ANOVA and pairwise t-tests.

For high-accuracy automatic pancreatic segmentation, a different two-phase method was developed by Dogan et al. [26] using CT images. The developed ap-

proach involves two steps: (1) Pancreas Localization, where The Mask R-CNN model is used to identify the approximate pancreatic location on the 2D CT slice, and (2) Pancreas Segmentation, where the candidate pancreatic area is further refined with 3D U-Net on the 2D sub-CT slices created in the first stage to produce the segmented pancreas region.

To detect key characteristics and malignant growths in the pancreas in the CT images, Dinesh et al. [27] developed a deep learning-based approach for predicting pancreatic cancer at an early stage. CNN and YOLO model-based CNN (YCNN) are developed in this paper. Images of pancreatic cancer are predicted using the CNN model. Additionally, to help with classification, we employ the CNN (YCNN) built on the YOLO concept. The threshold parameters booked as markers are used for predicting the proportion of pancreatic cancer feasts and key CT scan characteristics.

Most of the existing research on PDAC detection and segmentation produces better results. However, it has some difficulties such as (i) Due to the enormous number of images needed for model training, a lot of computer memory is needed to prevent model crashes when the memory load is exceeded, (ii) additional time for training and highly complex process, and (iii) The segmented image quality is poor. To overcome these difficulties, we propose a new, effective hybrid deep learning network model in this research.

3. PROPOSED METHODOLOGY

3.1. DATASET DESCRIPTION

Model testing was conducted using two accessible abdominal CE-CT datasets that combined images from the portal venous phase: (1) From Memorial Sloan Kettering Cancer Centre in Manhattan, New York, the training set is created for "The Medical Segmentation Decathlon" pancreatic dataset. It has pancreas and lesion voxel-level annotations as well as 281 patients with pancreatic malignancies [32], and (2) From the

Clinical Centre at the National Institutes of Health in the US, 80 people with a healthy pancreas are included in the "Cancer Imaging Archive" dataset, along with corresponding voxel-level annotations [33].

3.2. IMAGE ACQUISITION AND LABELING

Five scanners were used to get the CE-CT scans. The available image sizes were 1024 x 1024 pixels (10 images) or 512 x 512 pixels (232 images), and the slice thickness ranged from 1.0 to 5.0 mm. Images with a resolution of 1024 x 1024 were downsampled to 512 x 512 before being used in the model creation. With 17 years of experience, a pancreatic radiologist in abdominal radiology evaluated and corrected all segmentations. The pancreatic duct, pancreas parenchyma, and tumor were all segmented in the annotations.

3.3. AUTOMATIC PDAC DETECTION FRAMEWORK

For automatic PDAC diagnosis and localization, this work employs a segmentation-oriented method. In the proposed pipeline, the cutting-edge, effective automatic medical image segmentation network known as IDRCNN is used to develop the proposed model. The inference pipeline is depicted schematically in Fig. 1 from the initial picture input to the tumor.

For the non-PDAC and PDAC cohorts, pancreas-related manually extracted regions of interest (ROIs) are identified from the other anatomical features, training the anatomy segmentation network for separating the pancreas with the help of the PDAC cohort's reconstructed ROIs from images. From the non-PDAC cohort, ROIs are automatically annotated by this network. With the manually annotated PDAC cohort, these non-PDAC cohorts are subsequently combined for training the three different IDRCNN models in the process of PDAC detection. The three different networks are (1) segmentation of tumor only (IDRCNN_T), (2) segmentation of tumor and pancreas (IDRCNN_TP), and (3) segmentation of Pancreatic Duct (IDRCNN_PD).

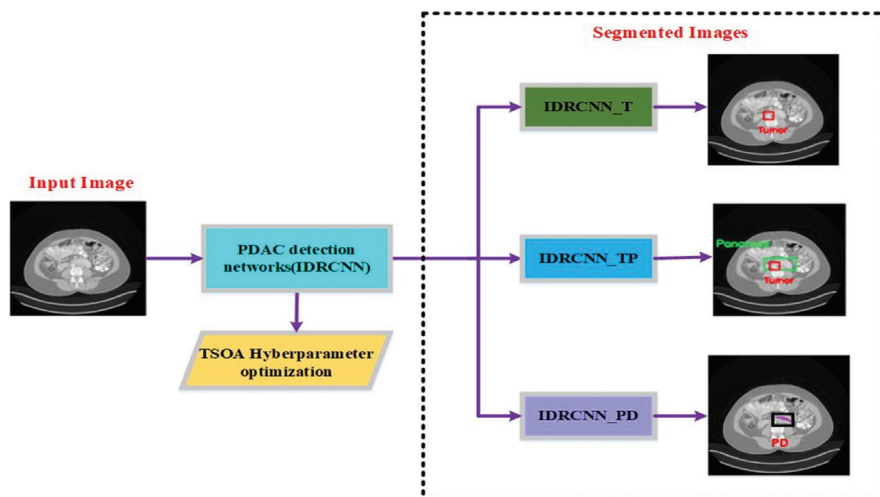


Fig. 1. An illustration of the proposed architecture for automatic PDAC detection

The models were produced for each configuration using identical splits using five-fold cross-validation from these networks. The cross-entropy loss function is better suited for segmentation-oriented detection tasks. It is chosen by default in the IDRCNN framework; it was employed for the PDAC detection networks. Additionally, From the PDAC cohort, a low-resolution pancreatic segmentation network was trained using the complete CE-CT images that had been down-sampled to 256×256 . This was subsequently used during inference for extracting the pancreatic ROI automatically from hidden images. The segmented tumor images produced using models like IDRCNN_T, IDRCNN_TP, and IDRCNN_PD for PDAC detection display the image regions.

3.4. IDRCNN-TSOA BASED ON TRAINING AND CLASSIFICATION

In this research, the IDRCNN is applied for training and classifying data. The IDRCNN is often very effective at enhancing the classification process's reliability and accuracy. Several researchers have used CNN to recognize PDAC from the provided images. This shows how CNN has made considerable progress in image processing. One deep learning method that permits weights and biases to various elements of images is CNN. CNN performs better at classification and can extract the features automatically. In the area of computer vision, CNN offers more accurate classification. An advanced level of depth occurs due to the residual connection being established as the neural network gets deeper.

Deep residual networks address the difficulties of network degradation, vanishing gradients, and exploring gradients. To detect and localize PDAC lesions on CE-CT scans, IDRCNN is preferred. A loss function is produced during the IDRCNN process, and it can potentially reduce the detection's performance. The hyper-

parameters should be modified for loss function reduction. The TSO algorithm is combined with the IDRCNN approach to adjust the hyperparameters.

A residual network's usual design consists of various techniques and arranges the fundamental components, such as normalization of pooling, non-linear mapping, and convolution sequentially. As a result, the IDRCNN's mathematical observation is considered as $H(x)$. For fitting the residual mapping, the residual function learned is known as $F(x)$ and is shown in the equation below.

$$F(x) = H(x) - x \quad (1)$$

The output of a conventional CNN has been used to represent the final mapping's residual learning. In Eq. (2), the convolutional method of calculation can be expressed;

$$V_{ij} = f \left(\sum_m \sum_{h=0}^{H_{1-1}} \sum_{w=0}^{W_{1-1}} k_{jm}^{hw} V_{(1-1)m}^{(x+h)(y+w)} + b_{ij} \right) + b_{ij} \quad (2)$$

The convolutional kernel size is represented as H_{1-1} & W_{1-1} , the number of keyframes is represented as m , the maximum number of iterations is described as $(i \& j)$, and the linear coefficient is represented by k and b .

Each image must train a convolution kernel before performing convolution processing. In general, accuracy and over-fitting issues affect the entire network due to the network's calculation efficiency and training speed. Different feature extraction algorithms are used for obtaining high-level features, which are more accurate due to the deep network structure. Batch normalization (BN), which successfully eliminates gradient explosion and vanishing gradient, is added after each convolution layer. After a network has been modified to include a residual structure more suitable for solving these problems, the gradient is propagated more readily and effectively due to shortcuts. The IDRCNN network's structure is also shown in Fig. 2.

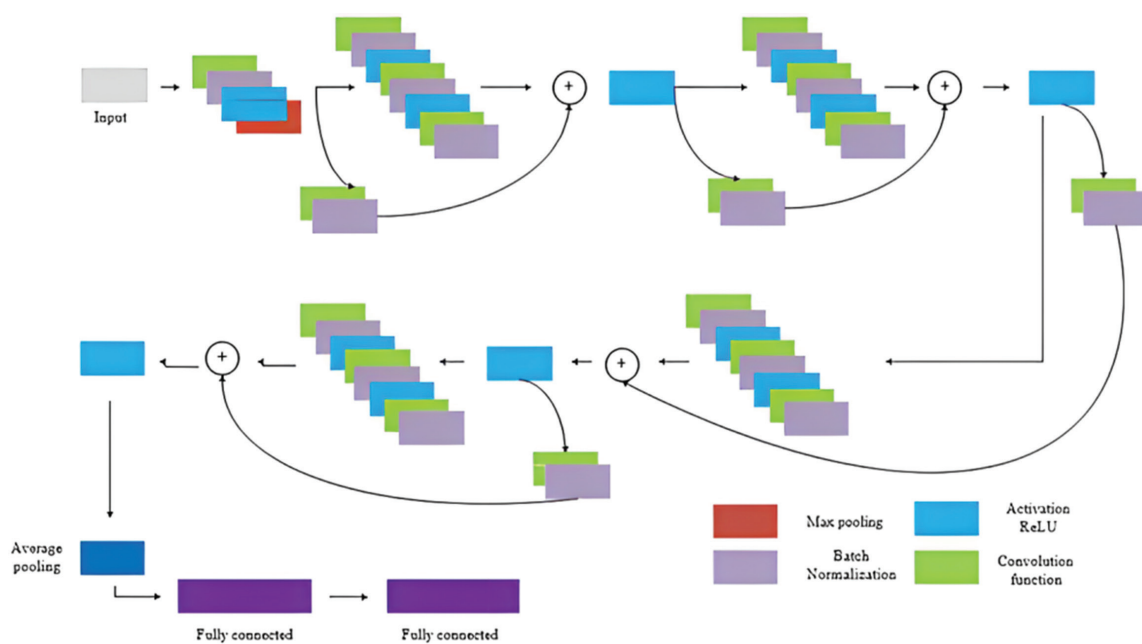


Fig. 2. The structure of the IDRCNN model

Internal parameters of the IDRCNN are optimized, and each layer's weight values are assigned to it. Another challenge in the network is the selection of hyper-parameters.

The selection domains $\Lambda_1, \Lambda_2, \dots, \Lambda_n$ of each hyperparameter are used to choose the assumed hyperparameters $\lambda_1, \lambda_2, \lambda_3, \dots, \lambda_n$. The model's domain space for selecting its hyper-parameters is then defined as $\Lambda = \Lambda_1 * \Lambda_2 * \dots * \Lambda_n$. Eq. (3) describes the hyperparameter optimization process;

$$f(\lambda) = \frac{1}{k} \sum L(\lambda, D_{train}^i, D_{valid}^i) \quad (3)$$

Where a loss of function is represented $L(\cdot)$, the training set is depicted as D_{train} , and the validation set is depicted as D_{valid} . Manual and grid search (violent search) are the two most used hyperparameter optimization techniques. However, optimizing for hyper-parameters has always been laborious since they could be more efficient. Because of how they are structured in a search area intended for automatic modification, hyper-parameters must be manually initialized. The images are finally divided into various classes using the Softmax classifier. This classifier works well for multi-class classification issues in general. The expression presented below defines the function of the Softmax layer.

$$S_i = \frac{e^{V_i}}{\sum_i^c e^{V_i}} \quad (4)$$

Where V_i represents the classifier's output value for class I , the number of classes is represented by c , and relative probability is defined by S_i . The method determines the relative likelihood of each type's output result, and the class's most significant relative probability group determines the classification outcomes.

3.5. HYPERPARAMETER OPTIMIZATION USING TSOA

TSO completed adjusting the IDRCNN's hyperparameter following the training and classification of data. The performance of the training approach is significantly impacted by the hyper-parameters, which are crucial for influencing the training approach's behavior. Due to the hyperparameter tuning, it was simpler to maintain a more significant number of experiments, and a better selection of hyperparameters resulted in a more efficient algorithm. In this suggested work, TSO is hybridized with IDRCNN to adjust the hyper-parameters of the classification algorithm. The TSO algorithm is one of the metaheuristic optimization algorithms with a bio-inspired design. During foraging and navigating, this algorithm simulates the actions of the swarm and jet populations of tunicates. The optimization strategy determines the ideal values by choosing the parameters for optimizing and describing the ranges to investigate. The ability of the tunicate to locate food sources has been described in the TSOA overview.

In this research, the food source has been considered as an optimization technique. Knowing the search term in the given search area is necessary for the suggested

optimization strategy to solve all optimization issues. For hyperparameter optimization, the IDRCNN uses the TSO algorithm as a result. When compared to selecting hyper-parameters manually, this optimization technique selects them quickly. This contributes to a better training process as well.

The number of iterations, position angle, wide angle, population size, and end condition have all been initialized by TSOA. Here, \vec{A} it is employed to determine the optimal position for the PDAC region while preventing conflict between the search agents.

$$\vec{A} = \frac{\vec{G}}{M} \quad (5)$$

$$\vec{G} = C_2 + C_3 - \vec{F} \quad (6)$$

$$\vec{F} + 2 \cdot C_1 \quad (7)$$

Where G represents the target function in Eq. (6), and the search agent's flow of advection is considered by F in Eq. (7). Then $C_1, C_2,$ & C_3 have been regarded as search agent variables; therefore, a force between the search agents are represented by \vec{M} , and Eq. (8) explains the calculation;

$$\vec{M} = [P1min_{maxmin}] \quad (8)$$

Where P_{maxmin} represents the minimum and maximum intensity iterations. Thus, the neighbor search agent's position is determined by using Eq. (9);

$$\vec{P}D = |\vec{F}S - r_{and} \cdot \vec{P}p(x)| \quad (9)$$

The tumor region's position is represented as $\vec{F}S$, the distance of the location is depicted as $\vec{P}D$, the position of the tunicate is expressed as $\vec{P}p(x)$, the current iteration is indicated as x , and the random number is considered as r_{and} in a wide range $[0, 1]$. The following equation in Eq. (10) has been calculated to keep the search agent in its position toward the best search;

$$\vec{P}p(x) = \begin{cases} \vec{F}S + \vec{A} \cdot \vec{P}D, & \text{if } r_{and} \geq 0.5 \\ \vec{F}S - \vec{A} \cdot \vec{P}D, & \text{if } r_{and} < 0.5 \end{cases} \quad (10)$$

Here, the search agent's updated position is $\vec{P}p(x)$. As well as being utilized for updating the tumor region's position and location, the behavior of the TSOA has been proposed as a means of fine-tuning the hyperparameter of the IDRCNN. As a result, the following equation in Eq. (11) has been used to determine the behavior of the TSOA as the best global search;

$$\vec{P}p(x+1) = \frac{\vec{P}p(x) + \vec{P}p(x+1)}{2 + C_1} \quad (11)$$

Additionally, the global position value has been regarded as the IDRCNN's weight updating where the hyperparameters' wide range of values is $[0, 1]$. The TSOA may also cover temporal and space complexity. The proposed pseudo-coding algorithm's TSOA has been calculated as follows;

Pseudo Code of IDRCNN-TSOA

Input: initialize the population size \vec{P}_p

Output: optimal fitness value \vec{F}_S

Initialize the hyperparameters $\{(\lambda_1, \lambda_2, \dots, \lambda_n), \vec{A}, \vec{G}, \vec{F}, \vec{M}\}$, and choose the Max number of iterations.

While ($x < m_{axiteration}$) **do**

for all hyper-parameters

 Compute fitness function (\vec{P}_p)

 Generate $r_{and}()$ with the range [0,1]

 Update the search agent's position using equation (11)

If ($r_{and} \leq 0.5$) **then**

$\vec{F}_S + \vec{A} \cdot \vec{P}_D$

else

$\vec{F}_S - \vec{A} \cdot \vec{P}_D$

end if

 Update \vec{P}_p for the optimal solution until the best solution

end for

Update the hyper-parameters

$x \leftarrow x+1$

end while

Return optimized hyperparameter value

The proposed IDRCNN-TSOA model assists in the best possible detection and localization of PDAC lesions. At this stage, the IDRCNN technique detects PDAC and the TSO algorithm is used to hyper-tune the parameters to minimize the obtained loss function. Thus, using the provided input pictures, the proposed IDRCNN-TSOA technique successfully segments the tumor, the tumor and pancreas, and the pancreatic duct.

4. RESULT AND DISCUSSION

This section covers the many performance metrics utilized to assess the suggested strategy and contrast it with the recent related previous approaches. We display the results of our experimental study on how cost-sensitive learning affects categorization ability.

This research offers a thorough and systematic application of deep learning methods (CNN) for precisely identifying and segmenting PDAC. Hybrid deep-learning models were used to classify and segment the CT image collection. The segmentation of PDAC images is developed using the hybrid IDRCNN-TSOA model, where the network training is done by using 70% of the dataset, and network validation is performed by using 30% of the dataset. The i5 processor and 8 GB of RAM were the computer resources used to obtain the results on the Python platform.

4.1. PERFORMANCE METRICS

Recall, precision, sensitivity, specificity, and accuracy are performance metrics used to assess segmentation performance, given below.

$$Recall = \frac{TP}{TP+FN} \quad (12)$$

$$Precision = \frac{TP}{TP+FP} \quad (13)$$

$$Sensitivity = \frac{TP}{FN+TP} \quad (14)$$

$$Specificity = \frac{TN}{TN+FP} \quad (15)$$

$$Accuracy = \frac{TP+TN}{TN+FN+TP+FP} \quad (16)$$

For the PDAC diagnosis, the number of true positives is known as the TP. Similarly, false positives are represented as FP, the true negatives are represented as TN, and the false negatives are indicated as FN.

4.2. ANALYSIS

The receiver operating characteristic (ROC) curve is employed for assessing patient performance. The free-response receiver operating characteristic (FROC) curve was used to assess lesion performance. The false positive rate (1-specificity) and actual positive rate (sensitivity) are contrasted within the ROC analysis at various model output thresholds to determine the model's confidence in the presence or absence of a tumor, referred to as the tumor likelihood map's highest value. For every specific lesion prediction at different thresholds, the false positive rate versus the average number of true positives per image is plotted in the FROC analysis to determine whether the model correctly detected the lesion.

The trained models were individually applied to testing the three PDAC-detection settings to compare them. The partial area under the FROC curve (pAUC-FROC) and the area under the ROC curve (AUC-ROC) are then compared to determine whether there were any statistically significant changes. The statistical significance was determined at a level of 97.5% confidence. Each configuration's final performance was identified by combining the models' forecasts.

4.3. EXPERIMENTAL RESULTS

Table 1 displays the results of the internal five-fold cross-validation sets using the three different PDAC detection network setups. With an AUC-ROC of 0.993, IDRCNN_PD performs best at the patient level. All networks produce a similar pAUC-FROC for lesion localization, with IDRCNN_PD and IDRCNN_TP performing somewhat better than IDRCNN_T.

Table 1. Internal five-fold cross-validation for each setup using the AUC-ROC and pAUC-FROC metrics

Configuration	Mean AUC-ROC (95%CI)	Mean pAUC-FROC (95%CI)
IDRCNN_T	0.974	3.795
IDRCNN_TP	0.987	4.245
IDRCNN_PD	0.993	4.660

Fig. 3 displays the mean FROC and ROC curves produced for each PDAC detection network design using the external test set, which correspond to the 95% confidence intervals. These curves were produced for each configuration using the proposed IDRCNN model (with five-fold cross-validation). Compared to training with just tumor segmentation, the findings on the external test set demonstrate that incorporating the pancreas parenchyma has a clear advantage at the patient level. Both IDRCNN_TP and

IDRCNN_PD produced a significantly higher AUC-ROC than IDRCNN_T. The IDRCNN_TP and IDRCNN_PD networks performed identically, nevertheless. In contrast, the three FROC curves clearly distinguished themselves at the lesion level across the whole test set (Figure 3), with pAUC-FROC being significantly greater for IDRCNN_PD than for the other two configurations. For localizing PDAC lesions, this displays how the incorporation of surrounding anatomy improves the model's capabilities.

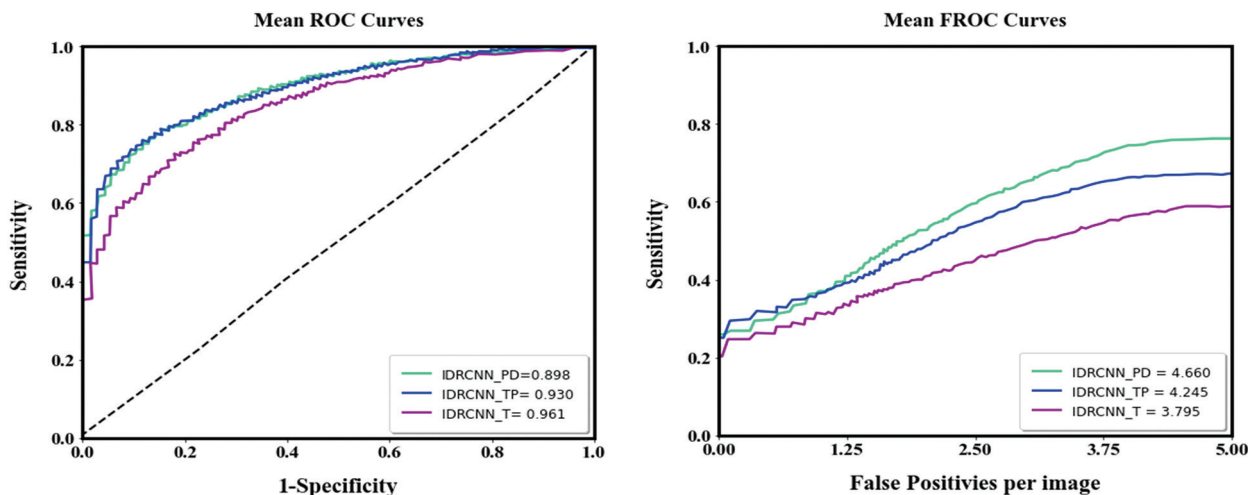


Fig. 3. Curves for the mean ROC and FROC for the external test set.

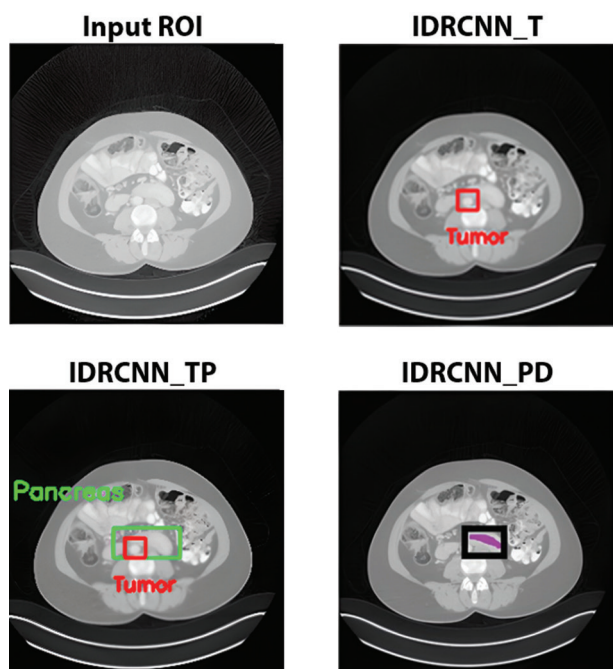


Fig. 4. Results of experiments using the proposed approach

In the instance of a pancreatic duct-obstructing iso-dense lesion, the benefit of anatomical integration is demonstrated in Fig. 4 and causes it to enlarge. Given that the tumor and healthy pancreatic parenchyma cannot be distinguished from one another, the IDRCNN_TP and IDRCNN_T models are unable to detect this lesion.

The dilated duct termination, however, allows IDRCNN_PD to locate its position in the pancreas precisely. In the pancreas parenchyma, the neural model can concentrate more on the remaining regions by the duct's segmentation through supervised training; this could be responsible for its capacity to identify small tumors. Additionally, the radiologist can interpret the network output regarding the tumor with the help of the multi-structure segmentation offered by IDRCNN_PD.

The proposed CNN architecture produces A high segmentation rate, making it the most efficient system for providing segmentation results based on CT images with the largest dataset of images used ever. The suggested model successfully extrapolates traits that describe the inter-scale heterogeneity of the illnesses, enhancing classification performance.

In the proposed segmentation network model, the residual connections make it easier to train deeper networks, which is crucial for capturing complex spatial relationships in images. The skip connections aid in the flow of gradients during backpropagation, making it feasible to train networks with many layers without suffering from vanishing gradients. Information from earlier layers can directly contribute to later layers, allowing the network to reuse essential features, which is beneficial for tasks like image segmentation, where different levels of features are necessary. Based on these advantages, our proposed IDRCNN segmentation network effectively segments the tumor region.

4.4. COMPARISON RESULTS

Our proposed model's PDAC identification findings are compared with those of earlier studies over CT images in this section. The performance comparison of the proposed and existing approaches are given in Table 2 regarding recall, precision, specificity, sensitivity, and accuracy.

This research created a completely automated system for finding and locating PDAC tumors on CE-CT images using the cutting-edge, self-configuring medical segmentation framework IDRCNN. The effect of incorporating surrounding anatomy was examined as well. Abdominal CE-CT images have only a small area for

the pancreas. And within that area, lesions are a much smaller target. These are used to make deep learning for PDAC detection extremely difficult. The entire CE-CT images would be exceedingly resource-intensive for training and testing the networks and offer practical information about the other organs. In this method, it is required to pick a low level of interest surrounding the pancreas. Still, it would take more time and resources to physically annotate the pancreatic before processing every image via the network, significantly reducing the model's clinical value. A smaller volume of interest is automatically extracted in the entire CE-CT images using our PDAC detection framework in the first step for solving this difficulty.

Table 2. Comparative analysis of proposed approach and state-of-the-art approaches

Reference	Method	Accuracy (%)	Recall (%)	Precision (%)	Sensitivity (%)	Specificity (%)
Mahmoudi et al. [23]	TAU-Net	87.36	88	82	-	-
Tureckova et al [28]	CNN	72.53	68	70	-	-
Si et al. [29]	FEE-DL	82.7	81.27	84.61	-	-
Qiu et al. [30]	MSTA	86.02	-	-	87.39	91.12
Ma et al. [31]	CNN	95.47	-	-	91.58	98.27
Althobaiti et al. [37]	CNN-CTPCD	95.49	-	-	91.50	98.64
Khdhir et al. [38]	ALO-CNN-GRU	95	-	-	-	-
Proposed Approach	IDRCNN	98.67	97.26	98.52	97.65	98.45

For PDAC segmentation, TAU-Net and 2D attention U-Net were developed by Mahmoudi *et al.* [23]. From the whole CT volume, the pancreas region is localized by using a 3D-CNN architecture with the help of the original images 3D Local Binary Pattern (LBP) map in this paper. TAU-Net achieves 87.36% accuracy in detecting the PDAC. A CNN model with deep supervision and attention gates was studied by Tureckova *et al.* [26], and in this paper, PDAC is detected with an accuracy of 72.53%. End-to-end deep learning (FEE-DL) developed by Si *et al.* [27] achieves 82.7% accuracy in detecting PDAC. Qiu *et al.* [28] studied a new MSTa (multi-resolution-statistical texture analysis) system for PDAC, which achieves an accuracy of 86.02%. For PDAC classification, a powerful CNN model was developed by Ma *et al.* [29]. It achieves a specificity of 98.27%, a sensitivity of 91.58%, and an overall accuracy of 95.47% for plain scans. Using CT images, an optimal deep learning-based pancreatic tumor and non-tumor classification (ODL-PTNTC) model is developed by Althobaiti *et al.* [31], and it achieves an average sensitivity of 91.50%, specificity of 98.64%, and accuracy of 95.49 % for pancreatic disease classification. For CT image-based pancreatic tumor segmentation and classification, the Antlion Optimization-Convolutional Neural Network-Gated Recurrent Unit (ALO-CNN-GRU) model was developed by Khdhir *et al.* [33], and it achieves an overall accuracy of 95% for pancreatic tumor classification. Our proposed IDRCNN model achieves a high performance with specificity of 98.45%, sensitivity of 97.65%, accuracy of 98.67%, recall of 97.26%, and precision of 98.52%.

Compared to the prior models, the proposed IDRCNN model achieves better results, and it effectively identifies the PDAC and segments the region of the tumor, pancreas, and pancreatic duct. The essential advantage of the proposed IDRCNN model is that it avoids overfitting and has no detrimental effects on network performance due to the classification and segmentation process.

The proposed DRCNN model optimizes the flow of information through both convolutional and residual connections; it could lead to improved gradient flow during training. This could result in faster convergence and better generalization performance than CNN models. In the TAU-Net model, the texture attention mechanisms can introduce additional computational complexity and memory requirements. This might result in slower training and inference times, making the architecture less suitable for real-time applications or resource-constrained environments. Still, our proposed approach utilizes minimum memory requirements and low computational complexity. The quality of the input images influences the effectiveness of multi-resolution analysis. Poorly captured images, noise, or artifacts can affect the accuracy of texture analysis at different scales. Hence, our proposed approach produces defective lesion regions with high-quality images during segmentation.

The end-to-end automatic diagnosis is performed by the proposed system, which is a significant advantage of this research, and the time it takes for each patient to

obtain a diagnosis after entering the initial abdomen CT image is 18.6 seconds. It is appropriate for clinical usage with significant promise for evaluating and recommending treatments since it can manage and usefully interpret vast volumes of data quickly, correctly, and affordably. The model, for instance, may be used to help diagnose patients in low-level hospitals with limited resources or for widespread pre-diagnosis during physical examinations. The model's capacity to generate saliency maps, highlighting the region's most crucial to its diagnostic decision-making, is a last feature that can increase its dependability. While clinicians have access to additional data, such as patient health records and testimony, our method only uses evidence from CT images. As a result, definitive diagnoses and treatment plans should still be based on the clinical evaluation of specialists, not just the output of a deep-learning system.

5. CONCLUSIONS

In CE-CT scans for tumor localizing, this research develops an effective and automatic deep-learning-based network model to localize the tumor in CE-CT scans and determine if a patient has PDAC. To precisely detect and localize PDAC tumors, the novel, effective IDRCNN model is employed. The maximum AUC of 0.961 is acquired by the proposed model, demonstrating that our proposed approach is an effective tool for recognizing tiny PDAC lesions and may help support radiologists in the early diagnosis of PDAC. In addition, we demonstrate that adding local anatomical information considerably improves model performance regarding lesion localization. The performance comparison demonstrates that while the proposed IDRCNN model adds a small amount of computing overhead, the performance is significantly improved. Finally, our automatic system has proven effective at detecting PDAC, making it more versatile than the current state of the art while still performing on a level with more specialized techniques.

In our future research, we will use the combination of two deep learning models for PDAC detection and also perform segmentation of several surrounding anatomical structures of the tumor.

Conflict of interests: The authors declare that they have no known competing financial interests or personal relationships that could have appeared to influence the work reported in this paper.

6. ACKNOWLEDGMENTS

We declare that this manuscript is original, has not been published before, and is not currently being considered for publication elsewhere.

Funding: No funding was received to assist with the preparation of this manuscript.

Availability of data and material: Data will be available when requested

Authors' contributions: The author confirms sole responsibility for the following: study conception and design, data collection, analysis and interpretation of results, and manuscript preparation.

Ethics approval: This material is the author's original work, which has not been previously published elsewhere. The paper reflects the author's research and analysis in a truthful and complete manner.

7. REFERENCE

- [1] Y. Fukuda, D. Yamada, H. Eguchi, T. Hata, Y. Iwagami, T. Noda, T. Asaoka, K. Kawamoto, K. Gotoh, S. Kobayashi, Y. Takeda, "CT density in the pancreas is a promising imaging predictor for pancreatic ductal adenocarcinoma", *Annals of surgical oncology*, Vol. 24, 2017, pp. 2762-2769.
- [2] H. Hayashi, N. Uemura, K. Matsumura, L. Zhao, H. Sato, Y. Shiraishi, Y. I. Yamashita, H. Baba, "Recent advances in artificial intelligence for pancreatic ductal adenocarcinoma", *World Journal of Gastroenterology*, Vol. 27, No. 43, 2021, p. 7480.
- [3] J. D. Kang, S. E. Clarke, A. F. Costa, "Factors associated with missed and misinterpreted cases of pancreatic ductal adenocarcinoma", *European Radiology*, Vol. 31, 2021, pp. 2422-2432.
- [4] R. P. Sah, A. Sharma, S. Nagpal, S. H. Patlolla, A. Sharma, H. Kandlakunta, V. Anani, R. S. Angom, A. K. Kamboj, N. Ahmed, S. Mohapatra, "Phases of metabolic and soft tissue changes in months preceding a diagnosis of pancreatic ductal adenocarcinoma", *Gastroenterology*, Vol. 156, No. 6, 2019, pp. 1742-1752.
- [5] W. Qiu, N. Duan, X. Chen, S. Ren, Y. Zhang, Z. Wang, R. Chen, "Pancreatic ductal adenocarcinoma: machine learning-based quantitative computed tomography texture analysis for prediction of histopathological grade", *Cancer Management and Research*, Vol. 11, 2019, p. 9253.
- [6] J. Chang, Y. Liu, S. A. Saey, K. C. Chang, H. R. Shrader, K. L. Steckly, M. Rajput, M. Sonka, C. H. Chan, "Machine-learning based investigation of prognostic indicators for oncological outcome of pancreatic ductal adenocarcinoma", *Frontiers in oncology*, Vol. 12, 2022, p. 6660.
- [7] T. Tong, J. Gu, D. Xu, L. Song, Q. Zhao, F. Cheng, Z. Yuan, S. Tian, X. Yang, J. Tian, K. Wang, "Deep learning radiomics based on contrast-enhanced ultra-

- sound images for assisted diagnosis of pancreatic ductal adenocarcinoma and chronic pancreatitis", *BMC Medicine*, Vol. 20, No. 1, 2022, pp. 74.
- [8] C. An, D. Li, S. Li, W. Li, T. Tong, L. Liu, D. Jiang, L. Jiang, G. Ruan, N. Hai, Y. Fu, "Deep learning radiomics of dual-energy computed tomography for predicting lymph node metastases of pancreatic ductal adenocarcinoma", *European Journal of Nuclear Medicine and Molecular Imaging*, Vol. 49, 2022, pp. 1187-1199.
- [9] Z. M. Zhang, J. S. Wang, H. Zulfiqar, H. Lv, F. Y. Dao, H. Lin, "Early diagnosis of pancreatic ductal adenocarcinoma by combining relative expression orderings with machine-learning method", *Frontiers in Cell and Developmental Biology*, Vol. 8, 2020, p. 582864.
- [10] L. C. Chu, S. Park, S. Kawamoto, Y. Wang, Y. Zhou, W. Shen, Z. Zhu, Y. Xia, L. Xie, F. Liu, Q. Yu, Application of deep learning to pancreatic cancer detection: lessons learned from our initial experience. *Journal of the American College of Radiology*, Vol. 16, No. 9, 2019, pp. 1338-1342.
- [11] S. Ziegelmayer, G. Kaissis, F. Harder, F. Jungmann, T. Müller, M. Makowski, R. Braren "Deep convolutional neural network-assisted feature extraction for diagnostic discrimination and feature visualization in pancreatic ductal adenocarcinoma (PDAC) versus autoimmune pancreatitis (AIP)", *Journal of clinical medicine*, Vol. 9, No. 12, 2020, p. 4013.
- [12] A. Patra, K. Panagiotis, G. Suman, A. Panda, S. K. Garg, A. Goenka, "Abstract PO-084: Automated detection of pancreatic ductal adenocarcinoma (PDAC) on CT scans using artificial intelligence (AI): Impact of inclusion of automated pancreas segmentation on the accuracy of 3D-convolutional neural network (CNN)", *Clinical Cancer Research*, Vol. 27, 2021.
- [13] G. A. Kaissis, S. Ziegelmayer, F. K. Lohöfer, F. N. Harder, F. Jungmann, D. Sasse, A. Muckenhuber, H. Y. Yen, K. Steiger, J. Siveke, H. Friess, "Image-based molecular phenotyping of pancreatic ductal adenocarcinoma", *Journal of Clinical Medicine*, Vol. 9, No. 3, 2020, p. 724.
- [14] W. Qiu, N. Duan, X. Chen, S. Ren, Y. Zhang, Z. Wang, R. Chen, "Pancreatic ductal adenocarcinoma: machine learning-based quantitative computed tomography texture analysis for prediction of histopathological grade", *Cancer Management and Research*, Vol. 11, 2019, p. 9253.
- [15] T. G. W. Boers, Y. Hu, E. Gibson, D. C. Barratt, E. Bonmati, J. Krdzalic, F. van der Heijden, J.J. Hermans, H.J. Huisman, "Interactive 3D U-net for the segmentation of the pancreas in computed tomography scans", *Physics in Medicine & Biology*, Vol. 65, No. 6, 2020, p. 065002.
- [16] T. A. Qureshi, C. Lynch, L. Azab, Y. Xie, S. Gaddam, S. J. Pandol, D. Li, "Morphology-guided deep learning framework for segmentation of pancreas in computed tomography images", *Journal of Medical Imaging*, Vol. 9, No. 2, 2022, p. 24002.
- [17] M. Kriegsmann, K. Kriegsmann, G. Steinbuss, C. Zgorzelski, A. Kraft, M. M. Gaida, "Deep learning in pancreatic tissue: Identification of anatomical structures, pancreatic intraepithelial neoplasia, and ductal adenocarcinoma", *International Journal of Molecular Sciences*, Vol. 22, No. 10, 2021, p. 5385.
- [18] C. Cen, L. Liu, X. Li, A. Wu, H. Liu, X. Wang, H. Wu, C. Wang, P. Han, S. Wang, "Pancreatic ductal adenocarcinoma at CT: a combined nomogram model to preoperatively predict cancer stage and survival outcome", *Frontiers in Oncology*, 2021, p. 1980.
- [19] M. A. Attiyeh *et al.* "Survival prediction in pancreatic ductal adenocarcinoma by quantitative computed tomography image analysis", *Annals of surgical oncology*, Vol. 25, 2018, pp. 1034-1042.
- [20] E. J. Koay *et al.* "A visually apparent and quantifiable CT imaging feature identifies biophysical subtypes of pancreatic ductal adenocarcinoma", *Clinical Cancer Research*, Vol. 24, No. 23, 2018, pp. 5883-5894.
- [21] H. Fu *et al.* "Automatic pancreatic ductal adenocarcinoma detection in whole slide images using deep convolutional neural networks", *Frontiers in oncology*, Vol. 11, No. 1, 2021, p. 665929.
- [22] T. A. Qureshi, S. Gaddam, A. M. Wachsmann, L. Wang, L. Azab, V. Asadpour, W. Chen, Y. Xie, B. Wu, S. J. Pandol, D. Li, "Predicting pancreatic ductal adenocarcinoma using artificial intelligence analysis of pre-diagnostic computed tomography images", *Cancer Biomarkers*, Vol. 33, No. 2, 2022, pp. 211-217.

- [23] T. Mahmoudi, Z. M. Kouzahkhanan, A. R. Radmard, R. Kafieh, A. Salehnia, A. H. Davarpanah, H. Arabalibeik, A. Ahmadian, "Segmentation of pancreatic ductal adenocarcinoma (PDAC) and surrounding vessels in CT images using deep convolutional neural networks and texture descriptors", *Scientific Reports*, Vol. 12, No. 1, 2022, p. 3092.
- [24] Y. Zhang, E. M. Lobo-Mueller, P. Karanicolas, S. Gallinger, M. A. Haider, F. Khalvati, "Improving prognostic performance in resectable pancreatic ductal adenocarcinoma using radiomics and deep learning features fusion in CT images", *Scientific Reports*, Vol. 11, No. 1, 2021, pp. 1-11.
- [25] F. Jungmann, G. A. Kaissis, S. Ziegelmayer, F. Harder, C. Schilling, H. Y. Yen, K. Steiger, W. Weichert, R. Schirren, I. E. Demir, H. Friess, "Prediction of tumor cellularity in resectable PDAC from preoperative computed tomography imaging", *Cancers*, Vol. 13, No. 9, 2021, p. 2069.
- [26] R. O. Dogan, H. Dogan, C. Bayrak, T. Kayikcioglu, "A two-phase approach using mask R-CNN and 3D U-Net for high-accuracy automatic segmentation of pancreas in CT imaging", *Computer Methods and Programs in Biomedicine*, Vol. 207, 2021, p. 106141.
- [27] M. G. Dinesh, N. Bacanin, S. S. Askar, M. Abouhawah, "Diagnostic ability of deep learning in detection of pancreatic tumour", *Scientific Reports*, Vol. 13, No. 1, 2023, p. 9725.
- [28] A. Turečková, T. Tureček, Z. Komínková Oplatková, A. Rodríguez-Sánchez, "Improving CT image tumor segmentation through deep supervision and attentional gates", *Frontiers in Robotics and AI*, Vol. 7, No. 1, 2020, p. 106.
- [29] K. Si, Y. Xue, X. Yu, X. Zhu, Q. Li, W. Gong, T. Liang, S. Duan, "Fully end-to-end deep-learning-based diagnosis of pancreatic tumors", *Theranostics*, Vol. 11, No. 4, 2021, p. 1982.
- [30] J. J. Qiu, J. Yin, W. Qian, J. H. Liu, Z. X. Huang, H. P. Yu, L. Ji, X. X. Zeng, "A novel multiresolution-statistical texture analysis architecture: radionics-aided diagnosis of PDAC based on plain CT images", *IEEE Transactions on Medical Imaging*, Vol. 40, No. 1, 2020, pp. 12-25.
- [31] H. Ma, Z. X. Liu, J. J. Zhang, F. T. Wu, C. F. Xu, Z. Shen, C. H. Yu, Y. M. Li, "Construction of a convolutional neural network classifier developed by computed tomography images for pancreatic cancer diagnosis", *World Journal of Gastroenterology*, Vol. 26, No. 34, 2020, p. 5156.
- [32] A.L. Simpson *et al.* "A large annotated medical image dataset for the development and evaluation of segmentation algorithms", *arXiv:1902.09063v1*, 2019.
- [33] Pancreas-CT, "The Cancer Imaging Archive (TCIA)", *Public Access-Cancer Imaging Archive Wiki*, Vol. 1, 2022.
- [34] Y. Bian, Z. Zheng, X. Fang, H. Jiang, M. Zhu, J. Yu, H. Zhao, L. Zhang, J. Yao, L. Lu, J. Lu, "Artificial intelligence to predict lymph node metastasis at CT in pancreatic ductal adenocarcinoma", *Radiology*, Vol. 306, No. 1, 2023, pp. 160-169.
- [35] K. Sekaran, P. Chandana, N. M. Krishna, S. Kadry, "Deep learning convolutional neural network (CNN) With Gaussian mixture model for predicting pancreatic cancer", *Multimedia Tools and Applications*, Vol. 79, No. 15, 2020, pp. 10233-10247.
- [36] T. Vaiyapuri, A. K. Dutta, I. H. Punithavathi, P. Durairam, S. S. Alotaibi, H. Alsolai, A. Mohamed, H. Mahgoub, "Intelligent deep-learning-enabled decision-making medical system for pancreatic tumor classification on CT images", *Healthcare*, Vol. 10, No. 4, 2022, p. 677.
- [37] M. M. Althobaiti, A. Almulihi, A. A. Ashour, R. F. Mansour, D. Gupta, "Design of optimal deep learning-based pancreatic tumor and nontumor classification model using computed tomography scans", *Journal of Healthcare Engineering*, Vol. 2022, 2022, pp. 1-15.
- [38] R. Khdir, A. Belghith, S. Othmen, "Pancreatic Cancer Segmentation and Classification in CT Imaging using Antlion Optimization and Deep Learning Mechanism", *International Journal of Advanced Computer Science and Applications*, Vol. 14, No. 3, 2023.